Applications in Energy and Combustion Science 9 (2022) 100047

Contents lists available at ScienceDirect

Applications in Energy and Combustion Science

journal homepage: www.sciencedirect.com/journal/applications-in-energy-and-combustion-science

Study on the influence of residence time on the componential evolution of biomass pyrolysis vapors during indirect heat exchange process through a combining method of bio-oil composition inversion and function fitting

Chu Wang, Rui Diao, Zejun Luo, Xifeng Zhu *

Department of Thermal Science and Energy Engineering, University of Science and Technology of China, Hefei, Anhui 230026, PR China

ARTICLE INFO

Keywords:
Biomass pyrolysis
Selective condensation
Vapor evolution
Non-condensable gasses
Function fitting

ABSTRACT

A novel and effective experimental method for describing the evolution curves and hot maps of biomass pyrolysis vapors with the adjustment of sweeping gas flow rate was developed during condensation. The composition proportion of pyrolysis vapors was inverted from the composition quantification of segmental bio-oil recovered by the specific condenser with two flumes. The mathematical relationship between location and vapor composition was fitted by Slogistic function. The condensable proportion of water decreased from 85% to 60% as N_2 flow rate increased from 100 mL/min to 500 mL/min under 340 K water bath. But 500 mL/min N_2 flow rate accelerated the disturbance of condensing field and improved the recoveries of components with stronger condensing abilities than water. The condensable proportion of guaiacol and its derivatives decreased from 60% to 40% under 300 mL/min but increased to 55% under 500 mL/min. Furthermore, the evolution difference between high-proportion and low-proportion components in pyrolysis vapors in the condensing field was also discussed as well as the unique evolution of components with azeotrope phenomenon or special solubility. For the first time, the adjustment mechanism of constant non-condensable components on the evolution of condensable components was clarified during water bath condensation, which would remarkably improve the comprehension for the complex phase transition process during the selective condensation of biomass pyrolysis vapors.

1. Introduction

The condensation of pyrolysis vapors was one of the core technologies for the bio-oil production from biomass pyrolysis and liquefaction [1]. The adjustment for condensation was a cheap and effective method to improve the quality of bio-oil in comparison with the optimization of feedstock or pyrolysis technique, which was convenient to the immediate application on the pilot-scale and commercial platforms of biomass pyrolysis and liquefaction [2]. Within the limited condensing capacity of condenser, the numerous components in biomass pyrolysis vapors exhibited various recovery effects because of the differences in their condensing abilities [3]. The competitive relationship between these components was observed during the liquefaction of pyrolysis vapors and the components with strong condensing abilities were preferred to condense [4]. Based on this competitive relationship the selective condensation technology was developed to achieve the online separation of pyrolysis vapors through setting the gradient multi-staged condensers in a complete condensing system. The separation and enrichment phenomenon of bio-oil components with fractional condensation was analyzed by the investigations of several scholars [5, 6]. However, these conclusions only considered the variation of bio-oil composition, but the actual condensing process simultaneously involved the frequent phase transitions of hundreds of compounds and how to study the componential evolution of pyrolysis vapors during condensation became the primary difficulty for the comprehension of condensing mechanism [7–9]. The component enrichment effect and adjustment precision of selective condensation would be improved significantly when the evolution mechanism of pyrolysis vapors was grasped in the condensing field.

Palla et al. attempted to describe the evolution and recovery of each component in high-temperature biomass pyrolysis vapors during indirect heat exchange through computational fluid dynamics (CFD) [10]. The modified Euler model was established for the numerical simulation of 12-component model compound of pyrolysis vapors. Compared with

* Corresponding author.
E-mail address: xfzhu@ustc.edu.cn (X. Zhu).

https://doi.org/10.1016/j.jaecs.2021.100047
Received 30 September 2021; Received in revised form 11 November 2021; Accepted 19 November 2021
Available online 22 December 2021

the experimental results under the similar conditions of pyrolysis and condensation, the simulated evolution results of guaiacol and coniferyl alcohol were coincident whereas the negligible recovery of acetic acid or propionic acid was far from the actual situation [4,11,12]. The incomplete model compound constitution of pyrolysis vapors and unknown thermophysical properties of complex components led to the partial difference between simulation and experiment, which was hardly revised by the current detection and identification technologies [13]. Therefore, the specialized experimental investigation was more likely to seize the true condensing mechanism of biomass pyrolysis vapors [9]. The vapor and liquid distribution measured by experimental methods was closely related to the actual distribution on the premise of reliable detection means. Ill et al. reported a dynamic phase equilibrium measurement for water activity in bio-oil based on Fourier transformed infrared spectrometer (FTIR) [14]. But the vapor-liquid distribution relationship of organic compounds would be not measured by this method because of the inaccurate quantification of FITR for organics [15]. Nevertheless, this study demonstrated the possibility on the inversion of condensable componential evolution in the condensing field from bio-oil components through effective experimental methods.

Assuming the negligible chemical reactions during condensation, we designed a unique and practicable experimental method for the evolution of biomass pyrolysis vapors based on bio-oil composition inversion and function fitting [16–18]. The bio-oil from different positions of condensing field was recovered segmentally and the local composition proportion of pyrolysis vapors was inverted from bio-oil composition at the corresponding location. The evolution curves and distribution heat maps of condensable components in the condensing field were described by selecting suitable function to fit the relationship between vapor composition and location. The predictive effectiveness of this method was verified after the condensing field was adjusted, and the description precisions of linear and nonlinear functions were distinguished for the evolutions of different components [18]. With the assistance of this method the evolution distributions of water, acetic acid, furfural and guaiacol in walnut shell pyrolysis vapors were investigated in a vertical tubular heat exchanger at 273–353 K water bath temperatures, which particularly revealed the recovery situation of condensable components along with the condensing field including the initial point of condensation as well as the variation tendency and peak point of recovery rate [16]. Besides water bath temperature, however, the condensation and recovery of biomass pyrolysis vapors during indirect heat exchange were also affected by sweeping gas flow rate and flow field shape and other factors [3]. Among them, sweeping gas flow rate was a more sensitive adjustment that exhibited better economy and quicker feedback time than water bath temperature [19]. But the recovery evolutions of pyrolysis vapors with changing sweeping gas flow rate were seldom studied due to lack of dependable research methods previously.

Furthermore, although the existing investigations summarized the influence of sweeping gas flow rate on bio-oil yield and composition, the individual impact on biomass pyrolysis or vapor condensation was not distinguished [6,20]. The study of Huang et al. reported that bio-oil yield increased first and then decreased with increasing inert gas flow rate in a fluidized bed reactor [21]. The suitable increase in flow rate decreased the residence time of pyrolysis products in the hot zone and avoided some secondary reactions while the extreme increase led to the eddy appearance in the flow field that would promote the secondary reactions of pyrolysis products. Therefore, for exclusively studying the influence of sweeping gas flow rate on condensation, the pyrolysis reactor should have the ability to avoid the significant effect of sweeping gas flow rate on biomass pyrolysis process. The previous results from our study indicated that the dense pile of pyrolysis feedstock generated the relatively saturated secondary reactions in the laboratory-scale fixed bed biomass pyrolysis reactor based on a horizontal tubular furnace, and the secondary reactions were negligibly affected by changing sweeping gas flow rate [22]. For developing the adjustment methods of selective condensation and reducing the production costs, the gap should be filled in the individual effect of sweeping gas on the evolution of pyrolysis vapors during condensation. In the present study, the novel and effective experimental method based on bio-oil composition inversion and function fitting was applied to investigate the effect of sweeping gas flow rate on the evolution of pyrolysis vapors during condensation. The liquefaction of walnut shell pyrolysis vapors was conducted in the specific condenser with two flumes for segmental bio-oil recovery. Bio-oil organic composition was quantified by internal standard method. The evolution curves and heat maps of condensable components were described by fitting the relationship of remaining vapor proportion and position with Slogistic function. The visual description of biomass pyrolysis vapors was successfully achieved without numerical simulation. The evolutions of pyrolysis vapors under different N_2 flow rates were compared for the separation and purification of high value-added components.

2. Materials and methods

2.1. Materials

The present study selected the walnut shells from Anhui Province, China as pyrolysis feedstock to conduct the experiment of pyrolysis and liquefaction. The proximate analysis of walnut shells (dry basis) was analyzed according to Standard GB/T 28,731–2012. The weight percentages of moisture, volatile, ash and fixed carbon in walnut shells were 3.73 wt.%, 74.32 wt.%, 0.97 wt.% and 20.98 wt.%, respectively. The ultimate analysis of walnut shells (dry ash-free basis) was conducted using Elementary VarioEL-III element analyzer. The weight percentages of carbon, hydrogen, oxygen, nitrogen and sulfur were 52.62 wt.%, 5.67 wt.%, 41.26 wt.%, 0.34 wt.% and 0.11 wt.%, respectively. The values for fixed carbon and oxygen were calculated by difference.

2.2. Laboratory-scale biomass pyrolysis liquefaction platform

The pyrolysis and condensation experiment of walnut shells was conducted on the platform shown in Fig. 1. This laboratory-scale platform was made of three systems: sweeping gas transportation system, fast pyrolysis system and vapor condensation system. The composition of three systems was introduced in our previous studies [16,22]. Particularly, the two flumes for bio-oil segmental recovery were added on the inner wall of the first condenser. The locations of two flumes were

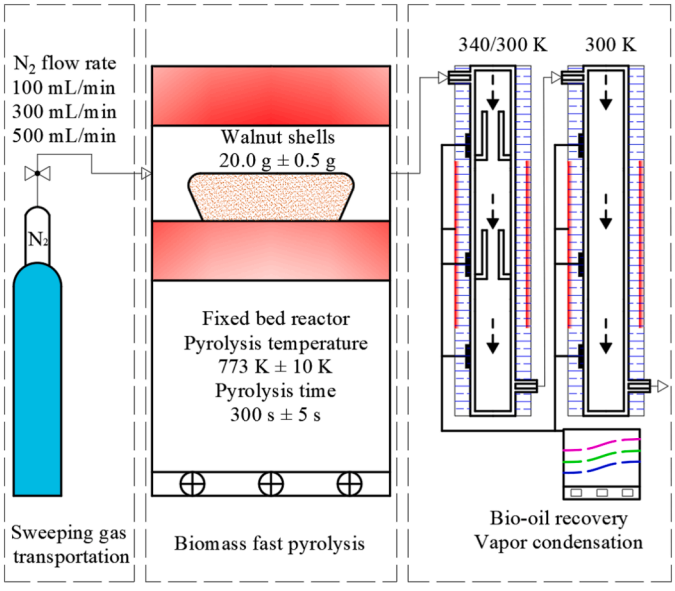

Fig. 1. Laboratory-scale platform for the pyrolysis and condensation experiment of biomass.

80 mm and 185 mm away from the vapor inlet of condenser. The reason for the specific positions of flumes was devoted to more distinct description at the beginning of fitted curve [16].

2.3. Experimental parameters

The maximum load of pyrolysis reactor was about 25 g walnut shells for each run, but the present study chose 20.0 $g \pm 0.5$ g walnut shells as pyrolysis feedstock for more sufficient heat exchange between reactor and biomass. The pyrolysis temperature was set at 773 $K \pm 10$ K that was proved to be the most suitable temperature for the pyrolysis and liquefaction of walnut shells on the present platform [18]. On the promise of about 20 g pyrolysis feedstock and 773 K pyrolysis temperature, 300 $s \pm 5$ s was verified to adequately pyrolyze these walnut shells in the present reactor [18]. The effect of 300–1500 mL/min N_2 flow rates on bio-oil composition was reported in our previous study [22]. The variation of sweeping gas in low flow rate range significantly affected the recovery of liquid products but high flow rate possibility damaged the air tightness of the whole device. Hence, N_2 flow rates were selected at 100 mL/min, 300 mL/min and 500 mL/min in turn for analyzing the evolution of pyrolysis vapors.

The present study was devoted to the evolution of biomass pyrolysis vapors with different sweeping gas flow rates in the single condensing field, from which the evolution could be extended in the continuous multi-staged condensing fields. Meanwhile, both extremely high and low water bath temperature tended to narrow the influential scope of sweeping gas flow rate, that had the potential to misunderstand the relevant effect mechanism. The investigation on the same platform indicated that the adjustment of sweeping gas flow rate showed the largest influential scope under 340 K water bath [22]. Thus, the present study set the water bath temperature at 340 $K \pm 1$ K and the primary target was the evolution variation of pyrolysis vapors under 340 K water bath. The second condenser was set at 300 $K \pm 2$ K (room temperature) for the recovery of valuable condensable components in the remaining vapors leaving the first condenser. For fitting evolution curve, the first condenser should also be set at 300 $K \pm 2$ K, at which negligible liquid products were recovered in the second condenser. All liquid products in the first condenser could be regarded as the total condensable components under the condensing capacity of water bath.

2.4. Bio-oil composition qualification

Because all bio-oil components were difficultly distinguished and qualified by the existing means especially large molecular oligomers and micro-content compounds, the typical components that could represent other components with similar structures and boiling points were preferred to be selected for investigation [13]. By comparing the values and features of detectable components, water, acetic acid, furfural, phenol, methyl cyclopentenolone (MCP), guaiacol, vanillin, 4-methyl guaiacol, catechol, 4-ethyl guaiacol, syringol and eugenol were selected for qualification [8]. The moisture in bio-oil was analyzed using Karl Fischer titrator. The internal standard method based on gas chromatography-flame ionization detector (GC-FID) was chosen to quantify the weight percentage (wt.%) of representative organic compounds in bio-oil. 1, 2, 4, 5-tetramethylbenzene was used as internal standard substance. The detailed method was given in our previous investigations [17,18].

2.5. Function fitting of vapor evolution

The evolution curves and heat maps of condensable components in biomass pyrolysis vapors with the development of condensing field were described through the combining method of bio-oil composition inversion and Slogistic function (Eq. (1)) fitting under the assumption of negligible chemical reactions during condensation [18]. As calculated by Eq. (2), the remaining vapor proportion (RVP) of one component denoted the relative percentage of vaporous component to the total component. M_0 was the total mass of one component recovered by the first condenser under 300 K water bath and M_i was the mass of one component recovered by flume i under 340 K water bath ($i \leq 3$). Flume 0 was the vapor inlet of condensing field and the theoretical value of M_0 was kept at 0, and flume 3 was the bottom of condensing field. The location of flume i was selected as 'x' of Slogistic function and the relevant RVP was selected as 'y' of Slogistic function, which was utilized to fit the vapor evolution curve of this component during condensation. The first derivative of fitted curve was named as recovery rate that represented the RVP decline per unit length of condensing field. The relevant parameters in the fitted equations were listed in Table 1.

$$y = \frac{a}{1 + e^{-k(x - x_c)}} \tag{1}$$

$$R_i = \frac{M_0 - \sum M_i}{M_0} \times 100\% \tag{2}$$

3. Results and discussions

3.1. Apparent behaviors of biomass pyrolysis and vapor condensation

Pyrolysis efficiency was calculated Eq. (3), which represented the weight percentage of total pyrolysis volatile to initial biomass feedstock [17]. Because of the negligible effect of sweeping gas flow on biomass pyrolysis in the present reactor, the similar pyrolysis efficiencies and feedstock masses proved that the components and proportions of pyrolysis vapors entering the condensing field were consistent with each other in all experiments (Fig. 2). As the segmental flumes were installed in the first condenser, unavoidable bio-oil adherence was observed on the inner wall after the liquid products were extracted from the first condenser. For comparing the degree of bio-oil adherence in different experiments, adherent rate was defined as the weight percentage of adherent bio-oil to total recovered liquid products (Eq. (4)) [17]. All adherent rates were maintained at about 10 wt.%, and on the base of our previous works this result indicated that the composition quantifications of segmental bio-oil from different experiments could be compared with each other because of the small and similar adherent rates.

$$\text{Pyrolysis efficiency} = \frac{\text{Initial walnut shell mass} - \text{Bio} - \text{char mass}}{\text{Initial walnut shell mass}} \times 100\text{wt.}\% \tag{3}$$

$$\text{Adherent rate} = \frac{\text{Actual bio} - \text{oil recovery} \; - \; \text{Total bio} - \text{oil segmental recovery}}{\text{Actual bio} - \text{oil recovery}} \times 100\text{wt.}\% \tag{4}$$

$$\text{Condensing efficiency} = \frac{\text{Bio} - \text{oil yield in one}'\text{s condenser or flume}}{\text{Pyrolysis efficiency}} \tag{5}$$

Under the same pyrolysis condition, the condensable components in high-temperature biomass pyrolysis products were determined by

Table 1
Parameters in Slogistic equation used for the fitting of RVP evolution curves.

	Water			Acetic acid			Furfural		
	100 mL/min	300 mL/min	500 mL/min	100 mL/min	300 mL/min	500 mL/min	100 mL/min	300 mL/min	500 mL/min
a	122.9885	110.8333	118.5560	147.6805	111.1026	133.4557	1490.7540	1397.4040	148.0530
x_c	120.9526	184.9289	206.0954	118.1342	283.9441	189.8451	−1678.5700	−2865.2800	222.8167
k	−0.0116	−0.0116	−0.0081	−0.0062	−0.0075	−0.0058	−0.0016	−0.0009	−0.0034
R^2	0.98950	0.99840	0.99967	0.99990	0.99750	0.99928	0.99997	0.99999	0.99631
	MCP			Phenols			Guaiacols		
	100 mL/min	300 mL/min	500 mL/min	100 mL/min	300 mL/min	500 mL/min	100 mL/min	300 mL/min	500 mL/min
a	102.8313	99.4656	100.1348	104.0492	2117.5090	107.5599	138.4202	212.7478	123.2504
x_c	263.7307	358.4823	298.2314	243.8220	−4087.4400	356.2909	143.8749	−43.5883	203.6689
k	−0.0127	−0.0120	−0.0152	−0.0110	−0.0007	−0.0070	−0.0063	−0.0028	−0.0071
R^2	0.99889	0.97277	0.99754	0.97787	0.98292	0.99599	0.98615	0.99969	0.99968

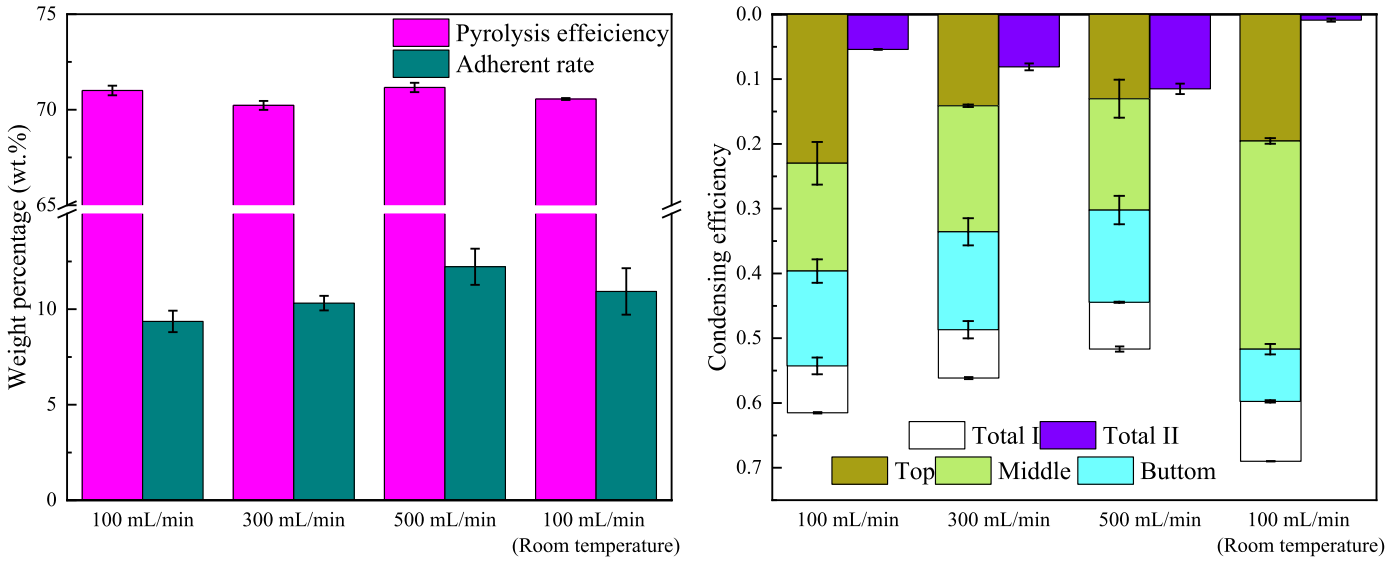

Fig. 2. Distribution of pyrolysis efficiency, adherent rate and condensing efficiency under different N_2 flow rates.

condensing condition. Poor heat exchange only allowed the condenser to recover some oligomers and sugars but most of pyrolysis products remained vapor, such as high-temperature oil bath and spraying. Remarkable heat exchange could even recover CO_2 and CH_4 that were non-condensable components under water bath, such as liquid nitrogen bath. For comparing the distribution of condensable and non-condensable components in the condensing field, the condensing efficiency was calculated by Eq. (5), which represented the ratio of the recoverable components in one flume or condenser to the total pyrolysis products [22]. Low condensing efficiency meant relative high proportion of non-condensable components in the current part of condensing field. High-temperature water bath would weaken the heat exchange between pyrolysis vapors and condenser and inhibit the liquefaction of low-boiling components with poor condensing abilities. At 100 mL/min N_2 flow rate, the total condensing efficiency of the first condenser increased from 0.62 to 0.69 when the water bath temperature decreased from 340 K to 296 K. The most increment of condensing efficiency was derived from the recovery improvement of the middle, which indicated that the recovery of high-temperature vapors in the top was hardly improved by decreasing water bath temperature because the limited space of top section was not enough to provide a relatively sufficient heat and mass exchange of pyrolysis vapors.

N_2 belonged to the constant non-condensable component within the adjustable temperature range of water bath, and the increasing N_2 would thicken the layer of non-condensable components that hindered the heat and mass exchange process in the condensing field. Thus, the total condensing efficiency of the first condenser decreased with increasing N_2 flow rate, and meanwhile most of increasing non-condensable components were recovered by the second condenser which kept its total condensing efficiency due to the strong condensing capacity from low water bath temperature. As N_2 flow rate was adjusted from 100 mL/min to 300 mL/min, the top condensing efficiency of the first condenser considerably decreased from 0.23 to 0.14 whereas the condensing efficiencies of middle and bottom section increased slightly. This finding indicated the condensation of top section was inhibited more seriously by increasing sweep gas due to the insufficient heat and mass exchange in the front part of condensing field. But 300 mL/min flow rate was difficult to completely inhibit the condensation of middle and bottom, and the components that failed to condense in the top were recovered in the middle and bottom, finally leading to the increment of local condensing efficiencies. When N_2 flow rate was further improved to 500 mL/min, the top condensing efficiency no longer showed a substantial decrease and the condensing efficiencies of three sections all decreased about 0.1–0.2 because of the enhancing inhibition. The distribution of condensing efficiency indicated that increasing N_2 flow rate exhibited a significant inhibition on the total recovery of liquid products. The flow rates lower than 300 mL/min mainly decreased the recovery effect of top section, and the inhibition phenomenon in the whole condensing field was eventually observed after the flow rate was further improved.

3.2. RVP evolution of representative components at different sweeping gas flow rates

3.2.1. Water

Water was the most widespread component in the pyrolysis products

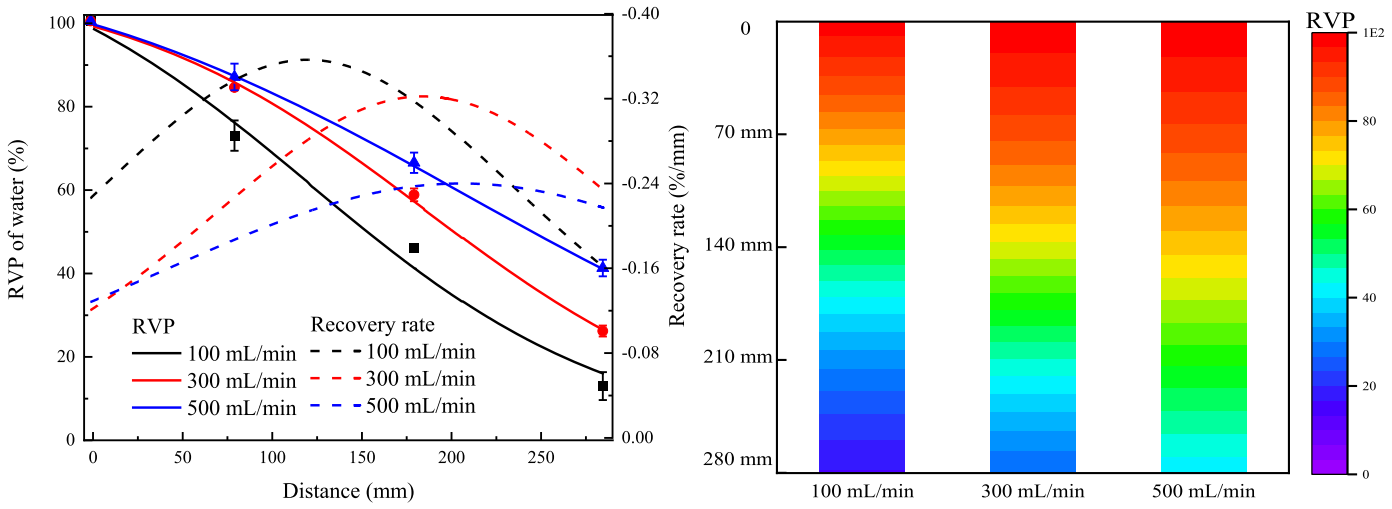

Fig. 3. Evolution curves and heat maps of water in biomass pyrolysis vapors during condensation.

of lignocellulosic biomass. The bio-oil with high moisture was usually produced by traditional biomass pyrolysis liquefaction technology, which brought a series of difficulties for the application and refinement of bio-oil. Hence, the separation of water from biomass pyrolysis vapors during liquefaction was the important mission of selective condensation [23]. Water belonged to the component hard to condense among the detectable components and exhibited the weakest condensing ability in the representative components. As shown in Fig. 3, the recovery rates of RVP evolution curves of water all presented the tendency of rise first and then fall along with condensing field at three N_2 flow rates. The consistent tendency was attributed to the poor condensing ability of water. The recovery of water was slowed at the vapor inlet with insufficient heat and mass exchange but increased with moving pyrolysis vapors in the condensing field due to the constantly accumulated chances of heat and mass exchange. However, the relative proportion of non-condensable components gradually increased as pyrolysis vapors moved to the middle and bottom of condensing field, which weakened the heat and mass exchange between water and condenser.

When N_2 flow rate increased from 100 mL/min to 300 mL/min under 340 K water bath, the initial recovery rate of water at the vapor inlet decreased from 0.23%/mm to 0.12%/mm and the final RVP of water at the end of condenser increased from 15% to 25%. Within 0–120 mm of condensing field, the two curves of recovery rates approximately kept parallel under 100 mL/min and 300 mL/min. The maximal recovery rate under 100 mL/min was observed at 140 mm away from the inlet of condensing field, whereas the location of the maximal recovery rate was delayed to 180 mm under 300 mL/min. After 175 mm, the recovery rate under 300 mL/min began to exceed the value under 100 mL/min because of the lower relative proportion of constant non-condensable components in the condensing field. When N_2 flow rate increased from 300 mL/min to 500 mL/min, the changeless recovery rate at the vapor inlet indicated that the inhibition of increasing N_2 flow rate on the water recovery of top condensing field was approximately saturated under 300 mL/min, and thereby the evolution curve in the top under 500 mL/min was coincident with the curve under 300 mL/min. After the mixture vapors entered the middle condensing field, the relatively serious inhibition on water recovery was observed under 500 mL/min and the maximal recovery rate was merely 0.23%/mm that was about 0.7 times as much as the peak value under 300 mL/min. Therefore, the final RVP of water under 500 mL/min was 1.6 times and 2.7 times as much as the final values under 300 mL/min and 100 mL/min, respectively.

With increasing N_2 flow rate in 285 mm vertical tubular condenser, the inhibition of the thickening layer of non-condensable components on water recovery reached saturation first in the top of condensing field, and the main section affected by this inhibition was transferred from the top and middle to the middle and bottom. For this reason, the RVP evolution curve of water under 300 mL/min decreased more slowly than that under 100 mL/min before 60% of the whole condensing field, while the curve under 500 mL/min decreased more slowly than that under 300 mL/min after 30% of the condensing field. At 340 K water bath temperature, the liquefaction and recovery of water were effectively reduced by promoting sweeping gas flow rate, which effectively decreased bio-oil moisture and achieved the online partial separation of water from organic compounds.

3.2.2. *Acetic acid*

Acetic acid accounted for a large proportion in the traditional pyrolysis liquefaction products of walnut shells that profoundly affected the bio-oil properties as well as the separation of high value-added components [24]. Although acetic acid presented a slightly stronger condensing ability than water, the actual recovery of acetic acid in the first condenser was lower than that of water. This finding possibly resulted from the adherence of some organic components on the condenser wall during the bio-oil transfer process from condenser to liquid storage tank. As a high-content component, acetic acid showed a stronger adhesion and the total mass of acetic acid in the recovered bio-oil was lower than the actual situation, which had been reported in our works. Therefore, the final RVP of acetic acid (Fig. 4) remained at about 40% under 100 mL/min and this value increased with increasing N_2 flow rate. Between acetic acid and water, the similar recovery rates in top section but the different recovery rates in middle and bottom section indicated that the primary adherence possibly occurred in the middle or bottom of condensing field. Generally, the bio-oil with low moisture was apt to adhere to wall because of large viscosity, but our previous study also found the serious adherence of bio-oil when high moisture led to the stratification of oil and water phases. In the present study, the moisture in the bio-oil recovered by the top was always maintained at 20 wt.% that provided good fluidity and homogeneousness for bio-oil, whereas the bio-oil recovered by the bottom exhibited a more visible stratification due to the moisture higher than 30 wt.%. Thus, the main reason for the high final RVP of acetic acid was the more serious adherence of acetic acid on the bottom wall.

As N_2 flow rate increased from 100 mL/min to 300 mL/min, the initial recovery rate of acetic acid was less than 0.10%/mm and the descent speed of evolution curve was slowed significantly. Although the total heat exchange of pyrolysis vapors increased with their movement in the condensing field, the maximal recovery rate of acetic acid merely reached to 0.21%/mm at the end of condenser, which was still less than the maximal recovery rate in the middle of condensing field under 100

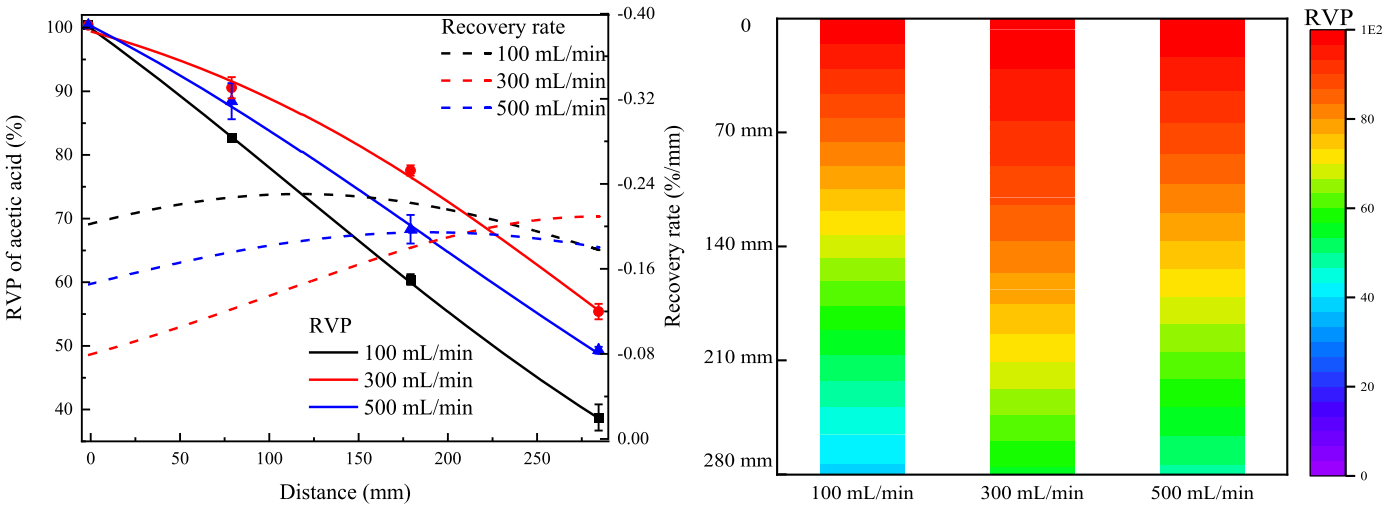

Fig. 4. Evolution curves and heat maps of acetic acid in biomass pyrolysis vapors during condensation.

mL/min. After the mixture vapors went through the first condenser under 300 mL/min, 55% of acetic acid remained vapor that was 1.4 times as much as the final RVP of acetic acid under 100 mL/min. Different from water, however, the RVP evolution curve of acetic acid was not further slowed but improved under 500 mL/min, and the initial recovery rate increased to 0.15%/mm. This phenomenon was because the disturbance of streamline was accelerated by 500 mL/min N_2, thus promoting the molecular collisions in pyrolysis vapors and improving the efficiency of heat and mass exchange during condensation. This improvement was relatively small and showed little effect on water with the weakest condensing ability, but the organic components with stronger condensing abilities than water could be affected effectively. Since the condensing ability of acetic acid was slightly higher than that of water, the final RVP of acetic acid under 500 mL/min only decreased about 5% from the final value under 300 mL/min.

The recovery of acetic acid would be inhibited by increasing sweeping gas flow rate, but the recovery of acetic acid under the condition of large flow rate was improved since the increasing disturbance of streamline promoted the intensification of heat and mass exchange of pyrolysis vapors. Overall, due to the relatively weak condensing ability, the total recovery of acetic acid under 500 mL/min successfully decreased about 10% in comparison with the result under 100 mL/min. Increasing N_2 flow rate to 500 mL/min could still be regarded as an effective method for the separation of acetic acid from pyrolysis vapors.

Table 2
Content distribution of representative components in segmental bio-oil under three N_2 flow rates.

		100 mL/min		300 mL/min		500 mL/min	
	Unit: wt.%	Content	± Err	Content	± Err	Content	± Err
Water	Top	20.82	2.75	19.90	0.27	17.86	4.25
	Middle	28.18	0.82	23.32	1.39	20.84	2.48
	Bottom	39.44	3.97	38.14	1.53	30.86	2.43
Acetic acid	Top	22.37	0.74	20.41	3.49	26.48	6.29
	Middle	38.79	1.45	19.65	1.23	33.97	3.78
	Bottom	43.03	4.08	43.13	2.36	38.74	1.11
Furfural	Top	1.73	0.07	1.66	0.42	2.04	0.34
	Middle	2.57	0.03	1.37	0.20	2.91	0.30
	Bottom	2.72	0.31	1.73	0.19	2.89	0.26
MCP	Top	0.13	0.03	0.20	0.09	0.15	0.04
	Middle	0.38	0.10	0.06	0.04	0.21	0.00
	Bottom	0.90	0.12	0.55	0.00	0.89	0.15
Phenols	Top	0.68	0.03	0.55	0.08	0.54	0.20
	Middle	0.68	0.20	0.23	0.09	0.50	0.05
	Bottom	2.28	0.36	0.44	0.08	1.22	0.03
Guaiacols	Top	4.85	0.37	4.80	0.23	5.63	1.33
	Middle	4.88	0.65	3.81	1.35	6.15	1.06
	Bottom	9.80	2.27	5.14	0.36	8.90	0.60

3.2.3. *Furfural*

As listed in Table 2, the total content of water and acetic acid was far higher than the total content of other organic compounds, which demonstrated that water and acetic acid belonged to high-proportion components while other detectable compounds belonged to low-proportion or trace-proportion components in walnut shell pyrolysis vapors. The comparison for evolution mechanisms was impractical between high-proportion and low-proportion components because of the considerable difference in their heat and mass exchange methods. Furfural was a component with weak condensing ability in the detectable low-proportion components. As the water bath temperature of the first condenser was set at 340 K, the final RVP of furfural in Fig. 5 was still more than 65% under 100 mL/min N_2 flow rate despite the macroscopical remarkable recovery of pyrolysis vapors. The high RVP of furfural indicated the recovery of furfural was considerably incomplete because of its weak condensing ability.

Under 100 mL/min, the recovery rate of furfural was 0.15%/mm at the vapor inlet but it did not exhibit an upward tendency with the movement of pyrolysis vapors in the condensing field. This result implied that the furfural recovery was not improved during the development of the total heat and mass exchange of mixture vapors possibly due to the existence of other factor affecting the condensation of furfural during indirect heat exchange rather than condensing ability. Previous investigation proved that furfural would present higher solubility in the liquid containing abundant acetic acid [25]. In the present study, the higher initial recovery rate of acetic acid promoted the initial recovery rate of furfural under 100 mL/min because of a larger proportion of acetic acid in walnut shell pyrolysis vapors and bio-oil. As the pyrolysis vapors was moving in the condensing field, the recovery rate of furfural decreased slightly with increasing relative proportion of non-condensable components. When N_2 flow rate increased to 300 mL/min, the initial recovery rate of furfural also decreased to 0.08%/mm with the substantial reduction of the initial recovery rate of acetic acid. The increasing proportion of non-condensable components inhibited the furfural recovery at the end of condensing field despite the high recovery rates of acetic acid. Thus, the recovery rate of furfural also showed a slightly downward tendency under 300 mL/min. As N_2 flow rate was set as 500 mL/min, the furfural recovery was significantly improved by the increasing recovery rate of acetic acid and the enhancing heat and mass exchange caused by high-frequency disturbance. The final RVP of furfural under 500 mL/min was consistent with

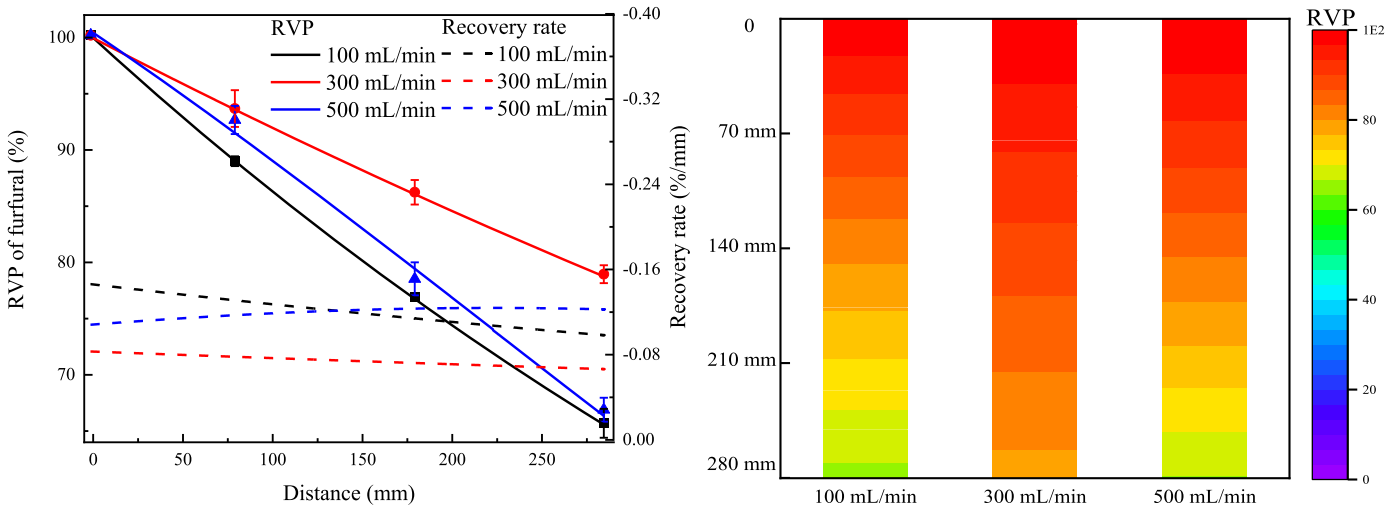

Fig. 5. Evolution curves and heat maps of furfural in biomass pyrolysis vapors during condensation.

that under 100 mL/min.

Under the three N_2 flow rates, the recovery rates of furfural evolution curves all exhibited narrow variations and the maximal recovery proportion of furfural was no more than 35%. As a high value-added component, furfural needed to be recovered more adequately. Significantly, 500 mL/min N_2 flow rate effectively inhibited the water recovery and improved the furfural recovery to the result achieved by 100 mL/min, which provided convenience for the separation and purification of furfural. Therefore, the small decline of water bath temperature for the condenser used to enrich furfural could further promote the furfural recovery with maintaining 500 mL/min N_2 flow rate. Meanwhile, a condenser at higher water bath temperature for separating the components with strong condensing abilities could be set in front of the condenser used to enrich furfural, which would also reduce the complexity of purifying furfural from bio-oil.

3.2.4. MCP

MCP was universally applied in food production and processing as a flavoring agent, and it presented the properties of olefin, carbonyl and hydroxyl together [26]. Hence, the condensing evolution mechanism of MCP was valuable to be studied despite the common content of MCP less than 1 wt.% in bio-oil (Fig. 6). According to the boiling point distribution of detectable components at normal atmosphere, MCP belonged to the component with middle condensing ability in all discussed components and exhibited a stronger condensing ability than furfural. The final RVP value of MCP was higher than that of furfural under each N_2 flow rate. However, the initial recovery rate of MCP was no more than 0.04%/mm that was merely approximate to the half of the minimal initial recovery rate of furfural. This finding was probably because the trace-proportion MCP in walnut shell pyrolysis vapors get little opportunity for heat and mass exchange in the top of condenser where the pyrolysis vapors contained abundant condensable components under the present condition of condensation. After the vapors moved to the middle of condensing field, the recovery rates of high-proportion components began to decrease whereas MCP exhibited a continuous increase in recovery rate because it was weakly affected by increasing non-condensable proportion by virtue of stronger condensing ability.

Under 100 mL/min, the recovery rate of MCP was about 0.04%/mm at the vapor inlet and gradually increased along with condensing field and reached the peak value of 0.32%/mm at the end of condensing field. The recovery proportions of MCP were 5%, 20% and 30% in the top, middle and bottom of condenser, respectively. As N_2 flow rate was improved to 300 mL/min, the initial recovery rate of MCP decreased to 0.015%/mm and the peak value of recovery rate decreased to 0.24%/mm due to the influence of increasing constant non-condensable proportion. In comparison with the result under 100 mL/min, the recovery proportions of MCP in the three sections all decreased by about half under 300 mL/min and the final RVP of MCP increased from 45% to

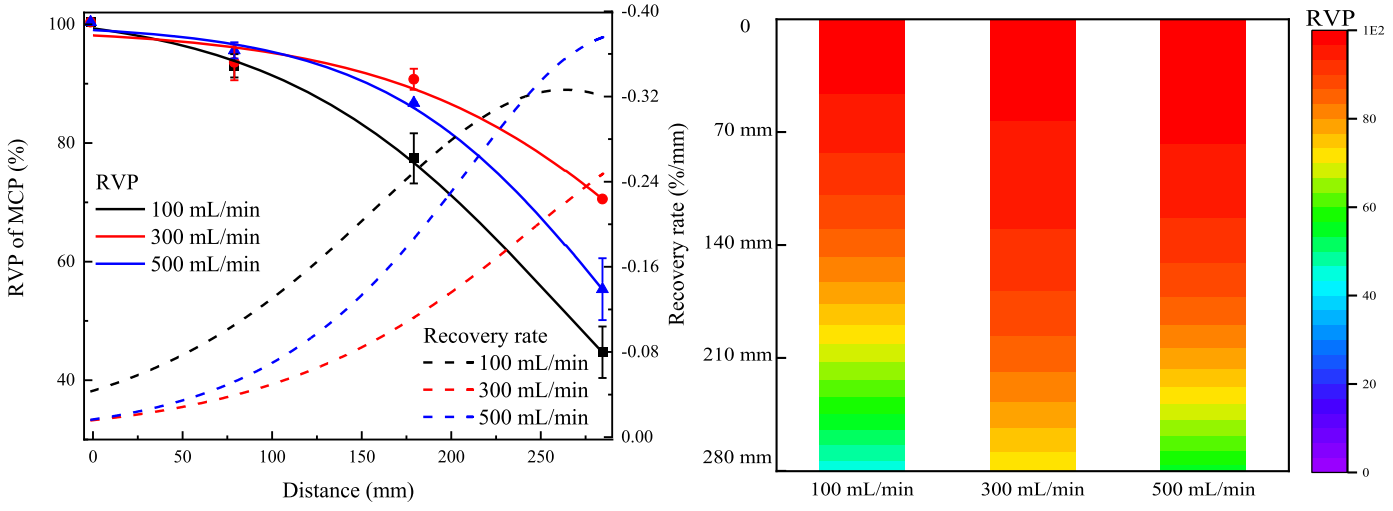

Fig. 6. Evolution curves and heat maps of MCP in biomass pyrolysis vapors during condensation.

70%. After the N_2 flow rate was further improved, the initial recovery rate was changeless but the ascensional range of recovery rate under 500 mL/min was far broader than that under 300 mL/min. The endmost recovery rate was 1.5 times as much as the value under 300 mL/min, which indicated that the improvement effect of 500 mL/min N_2 flow rate on MCP recovery was concentrated at the end of condensing field. As described in the evolution curves of MCP, the recovery proportions of top and middle varied negligibly but the bottom doubled the recovery proportion when N_2 flow rate increased from 300 mL/min to 500 mL/min.

The evolution curves of MCP revealed that the condensing priority of trace-proportion component was lower than that of high-proportion component in the condensing field under 340 K water bath but the trace-proportion component with stronger condensing ability was still recovered effectively in the bottom of condenser. Likewise, the high-frequency disturbance successfully improved the recovery of MCP under 500 mL/min flow rate. Nevertheless, 340 K water bath temperature showed a good recovery effect on water and specially the final RVP of water was less than 20% under 100 mL/min. If the recovery of MCP was required to be further strengthened, especially the improvement of its initial recovery rate, the recovery effect of condenser on high-proportion components with poor condensing abilities must be reduced. An appropriate increase in the water bath temperature outside the condensing field would effectively inhibit the recovery of high-proportion components and provide more opportunities for the heat and mass exchange of trace-proportion components with strong condensing abilities.

3.2.5. *Phenol and catechol*

Generally, walnut shells contained more than 50 wt. % lignin, and large amounts of phenolic compounds and pyrolytic oligomers were generated during the pyrolysis of abundant lignin [27]. As representative small-molecule phenolic compounds, the phenol and catechol (phenols) in walnut shell pyrolysis vapors were essential ingredients for medicine and chemical. At normal atmosphere, the boiling points of phenols were higher than that of furfural and the pure phenols showed stronger condensing abilities. Meanwhile, phenol or catechol also belonged to the trace-proportion component in walnut shell pyrolysis vapors. Therefore, the evolution curves for the RVP and recovery rate of phenols were consistent with those of MCP under 100 mL/min. The final RVP of phenols in Fig. 7 was slightly lower than that of MCP in 340 K condensing field, which proved phenols presented a stronger total condensing ability. In the composition of phenols, phenol exhibited a weaker condensing ability than MCP whereas the condensing ability of catechol was stronger than that of MCP. The above results indicated catechol dominated the total condensing ability of phenols under the present condition of condensation.

However, the evolution curve of phenols varied differently from MCP after N_2 flow rate increased. Under 300 mL/min, the recovery rate of phenols changed negligibly at the vapor inlet but decreased with the movement of pyrolysis vapors, and thereby the final RVP of phenols increased from 40 to 80%. This phenomenon proved that the extra inhibition effect on the recovery of phenols existed in the middle and bottom of condensing field under 300 mL/min. The investigation of Busca et al. reported that the azeotrope with weaker condensing ability was generated by the combination of water and phenol-structure compound [28]. The significant heat and mass exchange under 100 mL/min led to the sufficient recovery of water, phenols and their azeotrope together, while the decreasing heat and mass exchange under 300 mL/min was insufficient to recover the phenols because the generation of azeotrope was improved with ascending water in the mixture vapors. When N_2 flow rate was 500 mL/min, high-frequency disturbance promoted the recovery of phenols and azeotrope and improved the recovery rate of phenols in the bottom of condenser. At the end of condensing field, the recovery rate of phenols under 500 mL/min was 3 times as much as that under 300 mL/min and the final RVP of phenols decreased from 80% to 65%.

The evolution of phenols indicated that azeotropy also affected the competitive liquefaction process of biomass pyrolysis components based on their condensing abilities. The desired recovery of high-boiling component demanded to strength the heat and mass exchange between condenser and pyrolysis vapors when the target high-boiling component and low-boiling component formed the azeotrope with weaker condensing ability. The recovery under 100 mL/min was seldom influenced by azeotrope because of the sufficient condensing recovery of the overall pyrolysis vapors, but increasing azeotrope and decreasing heat and mass exchange synergistically decreased the recovery of target component under 300 mL/min. Fortunately, 500 mL/min sweeping gas flow rate increased the disturbance of condensing field and improved the recovery of azeotrope.

3.2.6. *Guaiacol and its derivatives*

Guaiacol and its derivatives (guaiacols containing 4-methyl guaiacol, 4-ethyl guaiacol, eugenol, syringol and vanillin) were high-boiling and large-molecule phenolic compounds in the detectable components of walnut shell pyrolysis vapors. As important fine chemical intermediates guaiacols could be utilized to synthesize flavor and medicine [29–31]. The content of each component of guaiacols was approximate to or more than 1 wt.% in all segmental bio-oil and the total content of detectable guaiacols was always approximate to or more than 5 wt.%. Hence,

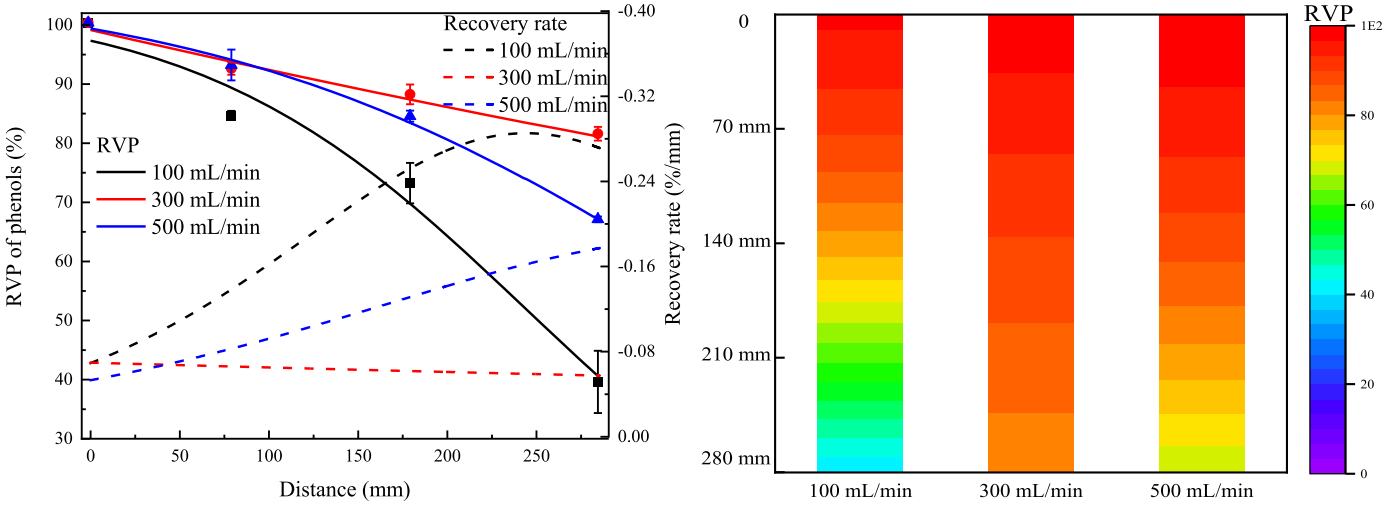

Fig. 7. Evolution curves and heat maps of phenols in biomass pyrolysis vapors during condensation.

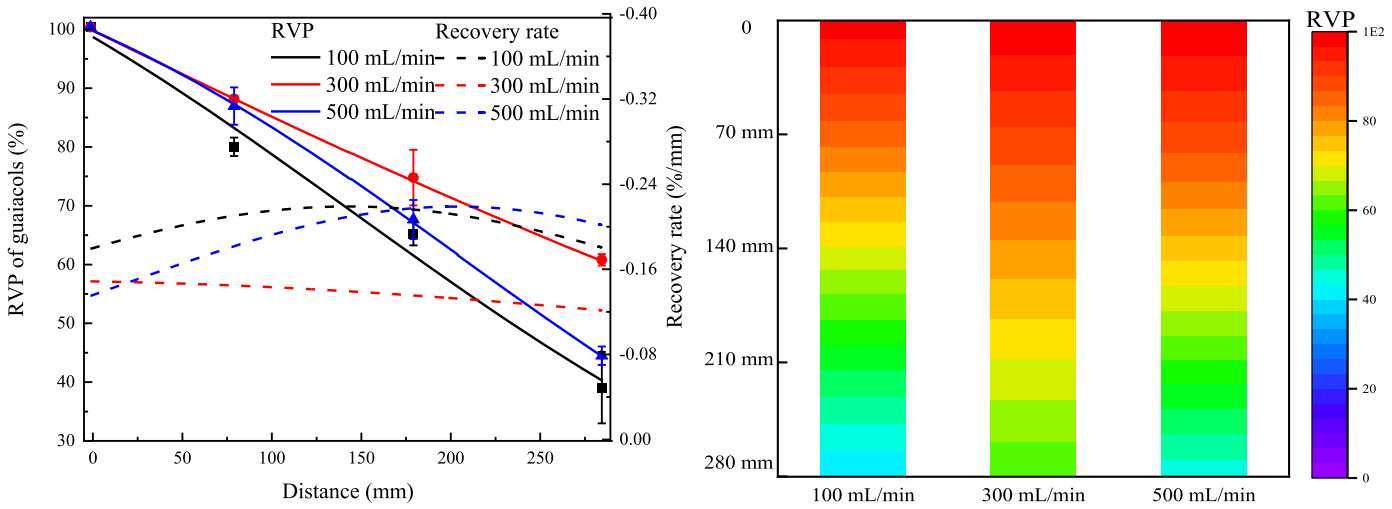

Fig. 8. Evolution curves and heat maps of guaiacols in biomass pyrolysis vapors during condensation.

guaiacols belonged to the low-proportion component in the pyrolysis vapors. The boiling points of guaiacols ranked first in the discussed components and thereby guaiacols presented considerably strong condensing abilities. In Fig. 8, the recovery rate of guaiacols under 100 mL/min was 0.18%/mm at the vapor inlet and exhibited a tendency of rising first and then falling along with condensing field. But the significant recovery of guaiacols at the vapor inlet limited the ascensional range of recovery rate because of their stronger condensing abilities and larger proportions in pyrolysis vapors than trace-proportion MCP and phenols.

When N_2 flow rate increased to 300 mL/min, the recovery rate of guaiacols decreased to 0.15%/mm at the vapor inlet and reached the peak value in the top of condensing field. As the relative proportion of non-condensable components increased in the condensing field, the recovery rate slightly decreased to 0.12%/mm at the end of condenser. The final RVP of guaiacols increased from 40% to 60%, but which was still higher than the final values of furfural, MCP and phenols under 300 mL/min because of the strong condensing abilities. Under 500 mL/min, the initial recovery rate decreased in comparison with that under 300 mL/min but the enhancing disturbance promoted the recovery of guaiacols in the middle and bottom of condensing field. The recovery rate reached the peak value of 0.21%/mm at 200 mm away from the vapor inlet under 500 mL/min whereas the same peak value occurred at 150 mm under 100 mL/min. The adjacent positions of peak value indicated that the recovery effect of condensing field on guaiacols under 500 mL/min was consistent with that under 100 mL/min. The two recovery curves of guaiacols under 100 mL/min and 500 mL/min primarily kept parallel in middle and bottom sections and the final RVP decreased to 45% under 500 mL/min.

Guaiacols presented the strong resistance to the inhibition of heat and mass exchange. At 340 K water bath temperature, the recovery rates of guaiacols with sufficient heat and mass exchange were maintained between 0.18 and 0.21%/mm under 100 mL/min while the decreasing recovery rates with poor heat and mass exchange were still maintained between 0.12 and 0.15%/mm under 300 mL/min. However, the recovery rate showed a significant upward tendency along with condensing field when 500 mL/min N_2 flow rate improved the condensation of pyrolysis vapors in the middle and bottom sections. The evolution results of guaiacols indicated that the heat and mass exchange enhancement under 500 mL/min could completely achieve the remarkable recovery effect of guaiacols, and simultaneously separate 20% of water and 10% of acetic acid from the recovered liquid products.

4. Conclusion

The suitable increment of N_2 flow rate inhibited bio-oil moisture and enriched the contents of organic compounds through increasing the high-frequency disturbance of condensing field. The incremental amount was determined by the property of condensable component. When N_2 flow rate increased from 300 mL/min to 500 mL/min, the final remaining vapor proportion of acetic acid with poor condensing ability only decreased from 55% to 50% while that of guaiacol and its derivatives with strong condensing abilities decreased from 60% to 45%. Despite poor condensing ability furfural exhibited a significant recovery at the vapor inlet due to the great solubility of furfural in high-content acetic acid. The recovery of phenol and catechol was considerably inhibited in the middle and bottom of condensing field because of the azeotrope formation between water and phenol-structure compounds.

Declaration of Competing Interest

The authors declare that they have no known competing financial interests or personal relationships that could have appeared to influence the work reported in this paper.

Acknowledgement

This work was supported by National Key Research and Development Program of China (2018YFB1501404).

References

[1] Sharifzadeh M, Sadeqzadeh M, Guo M, Borhani TN, Konda NVSNM, Garcia MC, et al. The multi-scale challenges of biomass fast pyrolysis and bio-oil upgrading: review of the state of art and future research directions. Prog Energy Combust 2019;71:1–80.
[2] Dalluge DL, Whitmer LE, Polin JP, Choi YS, Shanks BH, Brown RC. Comparison of direct and indirect contact heat exchange to improve recovery of bio-oil. Appl Energy 2019:251.
[3] Papari S, Hawboldt K. A review on condensing system for biomass pyrolysis process. Fuel Process Technol 2018;180:1–13.
[4] Sui HQ, Yang HP, Shao JG, Wang XH, Li YC, Chen HP. Fractional condensation of multicomponent vapors from pyrolysis of cotton stalk. Energy Fuel 2014;28:5095–102.
[5] Moutsoglou A, Lawburgh B, Lawburgh J. Fractional condensation and aging of pyrolysis oil from softwood and organosolv lignin. J Anal Appl Pyrol 2018;135:350–60.
[6] Ma SW, Zhang LQ, Zhu L, Zhu XF. Preparation of multipurpose bio-oil from rice husk by pyrolysis and fractional condensation. J Anal Appl Pyrol 2018;131:113–9.
[7] Papadikis K, Gu S, Bridgwater AV. Eulerian model for the condensation of pyrolysis vapors in a water condenser. Energy Fuel 2011;25:1859–68.

[8] Siriwardhana M. Fractional condensation of pyrolysis vapours as a promising approach to control bio-oil aging: dry birch bark bio-oil. Renew Energy 2020;152:1121–8.
[9] Tiarks JA, Dedic CE, Meyer TR, Brown RC, Michael JB. Visualization of physicochemical phenomena during biomass pyrolysis in an optically accessible reactor. J Anal Appl Pyrol 2019:143.
[10] Palla VSKK, Papadikis K, Gu S. A numerical model for the fractional condensation of pyrolysis vapours. Biomass Bioenerg 2015;74:180–92.
[11] Gooty AT, Li DB, Berruti F, Briens C. Kraft-lignin pyrolysis and fractional condensation of its bio-oil vapors. J Anal Appl Pyrol 2014;106:33–40.
[12] Papari S, Hawboldt K, Fransham P. Study of selective condensation for woody biomass pyrolysis oil vapours. Fuel 2019;245:233–9.
[13] Soria TM, Sanchez FA, Pereda S, Bottini SB. Modeling the phase behavior of cyclic compounds in mixtures of water, alcohols and hydrocarbons. Fluid Phase Equilibr 2014;361:143–54.
[14] Ille Y, Kröhl F, Velez A, Funke A, Pereda S, Schaber K, et al. Activity of water in pyrolysis oil – experiments and modelling. J Anal Appl Pyrol 2018;135:260–70.
[15] Zhou L, Zong ZM, Tang SR, Zong Y, Xie RL, Ding MJ, et al. FTIR and mass spectral analyses of an upgraded bio-oil. Energy Source Part A 2010;32:370–5.
[16] Wang C, Sun M, Deng J, Zhu X. Experimental study on composition evolution of biomass pyrolysis vapors with condensing temperature in a vertical tubular condenser. Bioresource Technol 2020:307.
[17] Wang C, Yang Y, Ma Y, Zhu X. Experimental study on the composition evolution and selective separation of biomass pyrolysis vapors in the four-staged indirect heat exchangers. Bioresource Technol 2021:332.
[18] Wang C, Huang Y, Diao R, Zhu X. Comparison of linear and nonlinear function to describe and predict componential evolution of biomass pyrolysis vapors during condensation in a tubular indirect heat exchanger. Bioresour Technol 2021;340:125654.
[19] Wu XM, Li T, Li QY, Chu FQ. Approximate equations for film condensation in the presence of non-condensable gases. Int Commun Heat Mass 2017;85:124–30.
[20] Kim P, Weaver S, Labbe N. Effect of sweeping gas flow rates on temperature-controlled multistage condensation of pyrolysis vapors in an auger intermediate pyrolysis system. J Anal Appl Pyrol 2016;118:325–34.
[21] Huang AN, Hsu CP, Hou BR, Kuo HP. Production and separation of rice husk pyrolysis bio-oils from a fractional distillation column connected fluidized bed reactor. Powder Technol 2018;323:588–93.
[22] Wang C, Luo ZJ, Li SY, Zhu XF. Coupling effect of condensing temperature and residence time on bio-oil component enrichment during the condensation of biomass pyrolysis vapors. Fuel 2020:274.
[23] Zhang L, Liu RH, Yin RZ, Mei YF. Upgrading of bio-oil from biomass fast pyrolysis in China: a review. Renew Sust Energy Rev 2013;24:66–72.
[24] Kan T, Strezov V, Evans TJ. Lignocellulosic biomass pyrolysis: a review of product properties and effects of pyrolysis parameters. Renew Sustain Energy Rev 2016;57:1126–40.
[25] Liu L, Chang HM, Jameel H, Park S. Furfural production from biomass pretreatment hydrolysate using vapor-releasing reactor system. Bioresource Technol 2018;252:165–71.
[26] Duan Y, Zheng M, Li DM, Deng DS, Ma LF, Yang YL. Conversion of HMF to methyl cyclopentenolone using Pd/Nb2O5 and Ca-Al catalysts via a two-step procedure. Green Chem 2017;19:5103–13.
[27] Zhao S, Wen J, Wang H, Zhang Z, Li X. Changes in Lignin Content and Activity of Related Enzymes in the Endocarp During the Walnut Shell Development Period. Hortic Plant J 2016;2:141–6.
[28] Busca G, Berardinelli S, Resini C, Arrighi L. Technologies for the removal of phenol from fluid streams: a short review of recent developments. J Hazard Mater 2008;160:265–88.
[29] Bolicke SM, Ternes W. Isolation and identification of oxidation products of syringol from brines and heated meat matrix. Meat Sci 2016;118:108–16.
[30] Kantar C, Kaya B, Turk M, Sasmaz S. Novel Phthalocyanines Containing Guaiacol Azo Dyes: synhthesis, Antioxidant, Antibacterial, and Anticancer Activity. J Struct Chem+ 2018;59:1241–50.
[31] Ma QY, Liu KJ, Mao JY, Chen KX, Liang C, Yao J, et al. Kinetic studies on the liquid-phase catalytic oxidation of 4-methyl guaiacol to vanillin. Can J Chem Eng 2017;95:1544–53.